Follicle outcomes in human ovarian tissue: effect of freezing, culture, and grafting

Camille Hossay, M.D.,[a] Francesca Tramacere, M.Sc.,[a] Luciana Cacciottola, M.D., Ph.D.,[a] Alessandra Camboni, M.D., Ph.D.,[a,b] Jean-Luc Squifflet, M.D., Ph.D.,[c] Jacques Donnez, M.D., Ph.D.,[d,e] and Marie-Madeleine Dolmans, M.D., Ph.D.[a,c]

[a] Gynecology Research Unit, Institut de Recherche Expérimentale et Clinique, Université Catholique de Louvain, Brussels, Belgium; [b] Anatomopathology Department, Cliniques Universitaires Saint-Luc, Brussels, Belgium; [c] Gynecology Department, Cliniques Universitaires Saint-Luc, Brussels, Belgium; [d] Society for Research into Infertility, Brussels, Belgium; and [e] Professor Emeritus, Université Catholique de Louvain, Brussels, Belgium

Objective: To study the effect of freezing, in vitro culture (IVC) and grafting to chorioallantoic membrane (CAM) on follicle outcomes in human ovarian tissue.
Design: An experimental study.
Setting: University-based research laboratory.
Patients: Fresh and cryopreserved ovarian tissue from 10 patients was donated to research with their consent and institutional review board approval.
Interventions: Fresh and frozen-thawed ovarian cortical pieces were in vitro-cultured and compared (fresh-IVC vs FT-IVC). The FT-IVC fragments were then examined against fragments grafted to CAM (FT-CAM). After both IVC and CAM grafting, ovarian cortical pieces ($4\times2\times1$ mm^3) were analyzed on days 0, 1, and 6.
Main Outcome Measures: Follicle analyses included histology (count and classification) and immunohistochemistry (Ki67 [proliferation], caspase-3 [apoptosis], 1A and 1B light chain 3B [autophagy], p-Akt, FOXO1, and p-rpS6 [PI3K activation]). Droplet digital polymerase chain reaction further explored expression of PI3K pathway- and oocyte-related genes in tissue sections.
Results: No major differences were detected between fresh-IVC and FT-IVC tissues in any conducted analyses. Although a significant drop was observed in primordial follicle (PF) proportions in the fresh-IVC and FT-IVC groups (d0 vs. d6, $P<.002$), they held steady in the FT-CAM group (d0 vs. d6, $P>.05$). The PF rates were also significantly higher in the FT-CAM group than the FT-IVC group on d6 ($P=.02$). Importantly, avian erythrocytes were already present in 30% of implants from d1. Apoptotic and autophagic follicle rates increased during IVC ($P<.008$), but remained significantly lower in the FT-CAM group ($P<.01$), confirming superior follicle preservation in CAM-grafted tissue. Upregulation of the PI3K/FOXO pathway was established in the IVC groups, demonstrating PF activation, whereas significant pathway downregulation was detected in the FT-CAM group ($P<.03$). The droplet digital polymerase chain reaction tests confirmed oocyte growth during IVC and follicle autophagy in all groups; however, the PI3K pathway appeared to be differentially modulated in tissues and follicles.
Conclusions: In vitro culture induces PF depletion with no additional impact of freezing. Grafting to CAM preserves the PF pool by curbing follicle activation, apoptosis, and autophagy, probably thanks to rapid graft revascularization and/or the circulating embryonic antimüllerian hormone. These findings highlight the importance of enhancing neoangiogenesis in ovarian grafts and investigating the potential benefits of administering antimüllerian hormone to prevent PF burnout. (Fertil Steril® 2023;119:135–45. ©2022 by American Society for Reproductive Medicine.)
El resumen está disponible en Español al final del artículo.

Key Words: Follicle activation, ovarian tissue cryopreservation, in vitro culture (IVC), chorioallantoic membrane (CAM)

Received May 10, 2022; revised September 23, 2022; accepted September 28, 2022.
Supported by grants from the Fonds National de la Recherche Scientifique de Belgique (Télévie grant 7.6511.20F awarded to C.H., F.R.S.-FNRS/FRIA FC29657 awarded to L.C., 5/4/150/5 grant and FNRS-PDR Convention grant number T.0077.14 awarded to M.M.D), the Fonds Spéciaux de Recherche, the Foundation Against Cancer (2018-042 awarded to A.C.) and private donations (Ferrero, Philippe de Spoelberch).
C.H. has nothing to disclose. F.T. has nothing to disclose. L.C. has nothing to disclose. A.C. has nothing to disclose. J.L.S. has nothing to disclose. J.D. has nothing to disclose. M.M.D. has nothing to disclose.
Correspondence to: Marie-Madeleine Dolmans, M.D., Ph.D., Gynecology Research Unit, Institut de Recherche Expérimentale et Clinique, Université Catholique de Louvain, Brussels, Belgium; and Gynecology Department, Cliniques Universitaires Saint-Luc, Avenue Mounier 52, bte. B1.52.02, 1200 Brussels, Belgium (E-mail: marie-madeleine.dolmans@uclouvain.be).

Fertility and Sterility® Vol. 119, No. 1, January 2023 0015-0282/$36.00

https://doi.org/10.1016/j.fertnstert.2022.09.360

Ovarian tissue cryopreservation and transplantation is an effective strategy for fertility preservation and restoration in patients having to undergo gonadotoxic therapies (1–4). However, massive depletion of the primordial follicle (PF) pool that occurs after transplantation limits graft longevity and, in turn, the effectiveness of the procedure (5–10). The PF pool constitutes the entire ovarian reserve (11–13). Its size and quality are principal determinants of fertility potential; therefore, it requires protection from direct follicle death and/or abnormal follicle activation related to stressful events like gonadotoxic treatments and hypoxic damage (4, 14).

Recruitment of PFs is normally regulated by highly controlled mechanisms that ensure a balance between quiescence and growth, preventing premature depletion of the ovarian reserve. The phosphoinositol-3-kinase (PI3K) signaling pathway is a known major network responsible for PF activation (15–17). Upon protein kinase B (Akt) phosphorylation by PI3K, a number of effectors are triggered, including forkhead box O (FOXO), tuberous sclerosis complex 1/2 (TSC1/2), and mechanistic target of rapamycin (mTOR). When located in the oocyte nucleus, FOXO acts as a transcriptional factor that suppresses follicle growth by promoting transcription of the cyclin-dependent kinase inhibitor 1B (*CDKN1B*) gene, among others. *TSC1* is an inhibitor of mTOR, but once phosphorylated, *TSC1* loses its inhibitory function and mTOR is activated. Moreover, mTOR is a conserved serine/threonine kinase and phosphorylates a series of proteins, including ribosomal protein S6 (rpS6) that promotes cell growth and regulates autophagy. The latter is a key biological process whereby cells dispose of unnecessary, dysfunctional, or damaged cellular components, ensuring either cell renewal in stressful conditions or cell death in the presence of excessive organelle damage (18, 19).

Massive follicle activation has been found to occur in similar ways after xenotransplantation and in vitro culture (IVC) of frozen-thawed human ovarian tissue through stimulation of the PI3K pathway (10, 20), raising the question of whether it is a consequence, at least in part, of the freezing procedure. Although a number of studies have indicated that cryopreservation is not responsible for the diminished follicle density observed after mid to long term grafting (8, 21–23), recent findings suggest that freezing accelerates follicle activation during IVC and differentially modulates the PI3K pathway in mouse ovaries (24).

Interestingly, previous studies using different animal ovarian tissues grafted to chick chorioallantoic membrane (CAM), whose constitution mimics the typical grafting site of peritoneum (25–27), showed inhibition of spontaneous follicle activation, with the PF reserve remaining intact for up to 10 days (28–31). However, its ability to preserve the PF pool has not yet been investigated in human ovarian tissue, and questions remain about the mechanisms through which it exerts its protective effects.

We hypothesized that IVC of human ovarian tissue would induce PF loss by increasing both follicle apoptosis and activation, and that freezing would aggravate these processes. By contrast, we assumed that grafting human ovarian tissue to CAM would preserve the ovarian reserve by reducing both follicle apoptosis and activation. Autophagy, a prosurvival response to stressful events, was also evaluated in follicles and was expected to intensify after freezing and IVC, and abate when tissue was grafted to CAM.

MATERIALS AND METHODS

Experimental Design

Thirty fresh cortical fragments were obtained from 5 patients (mean age, 29.14 years; range, 27.41–31.18) and 50 frozen-thawed cortical pieces from another 5 patients (mean age, 29.27 years; range, 27.96–30.91) for either IVC or grafting to CAM. All patients underwent laparoscopic surgery for non-ovarian diseases. We first compared fresh fragments (fresh-IVC) with frozen-thawed fragments (FT-IVC) across 0, 1, and 6 days of IVC to investigate the impact of freezing. Cultured frozen-thawed fragments were then further compared with frozen-thawed fragments grafted to CAM (FT-CAM) also for 0, 1, and 6 days to identify the differences between the IVC and CAM models.

Ethical Approval

Use of human tissue was approved by the *Institutional Review Board of the Université Catholique de Louvain* (n°2012/23MAR/125), and patients gave their written informed consent for the use of their ovarian tissue for research purposes.

Ovarian Tissue Cryopreservation and Thawing

Ovarian tissue cryopreservation was performed at the *Cliniques Universitaires Saint-Luc* using the slow-freezing protocol. Briefly, cryovials containing cortical fragments immersed in freezing medium composed of 10% dimethyl sulfoxide (DMSO, Sigma, Belgium) were placed in a programmable freezer (Kryo 10, Series III, Planer, UK), before being stored in liquid nitrogen (32). Thawing was done following a fast-thawing procedure, as previously described (32).

Biopsy Processing

Fresh biopsies were transferred to the laboratory on ice in MEM-GlutaMax (Gibco, Life Technologies, Belgium) and frozen biopsies were thawed. They were then dissected in 10 mL of pre-warmed dissection medium to remove any surplus medulla, as documented elsewhere (20). The biopsies were subsequently cut into cortical fragments of $4\times2\times1$ mm^3, with 2 fragments from each patient fixed for further evaluation as day 0 controls.

In Vitro Culture

Twenty fresh and 20 frozen-thawed strips were individually and randomly placed in 4-well culture dishes (Thermo Fisher, Belgium) filled with 300 μL pre-warmed culture medium (McCoy's 5a containing bicarbonate supplemented with 25 mM HEPES [Gibco], 0.1% human serum albumin [HSA; CAF-DCF, Belgium], 3 mM glutamine [Sigma], 30 μg/mL penicillin G [Sigma], 50 μg/mL streptomycin [Sigma], 2.5 μg/mL transferrin [Fisher Scientific], 4 ng/mL selenium [Sigma] and

FIGURE 1

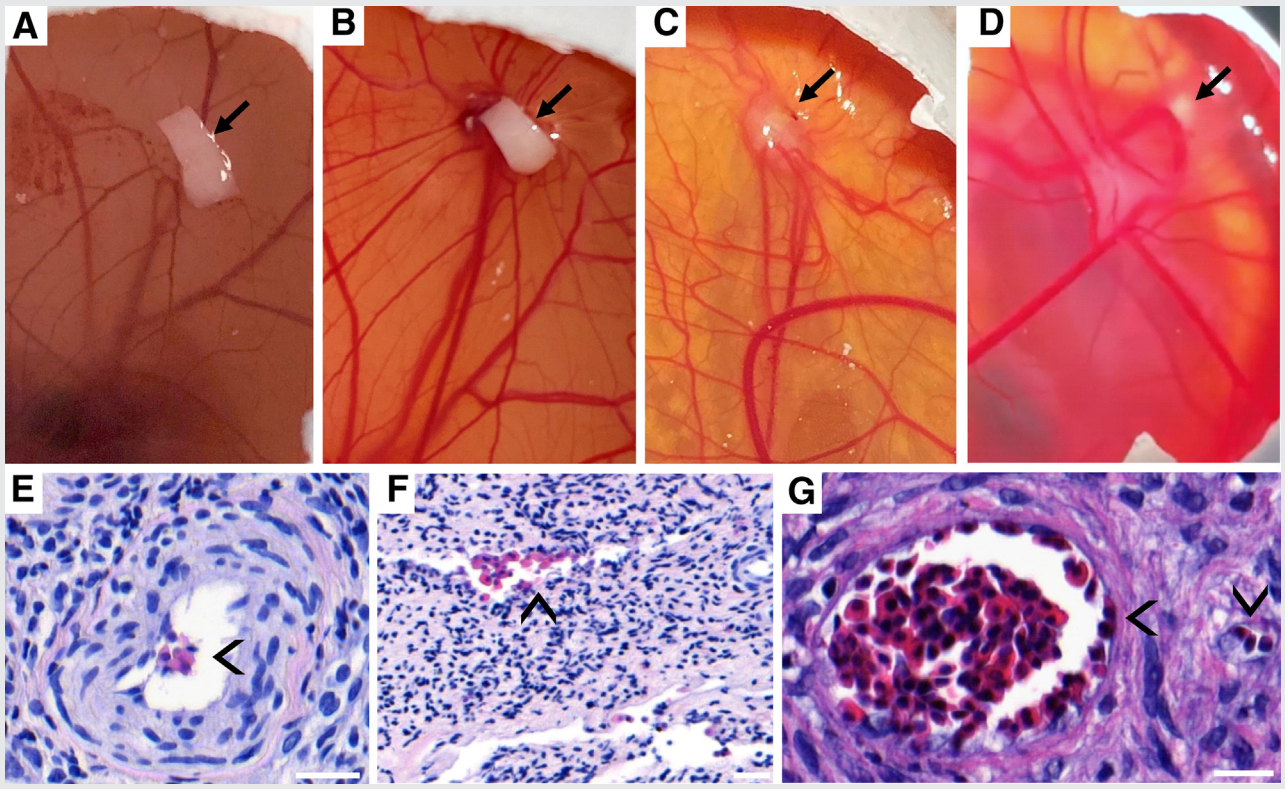

Macroscopic and microscopic evaluation of cryopreserved human ovarian tissue grafted to chorioallantoic membrane (CAM). Macroscopic aspect of ovarian tissue grafted to the traumatized CAM of a 7-day-old chick embryo on day 0 (**A**), day 1(**B**) and day 6 (**C**,**D**). Note the wheel-spoke pattern of CAM blood vessels around the ovarian graft on day 1 (**B**). By day 6, the grafts were covered with a second layer of CAM (**C**) and most of them penetrated the egg (**D**). Histology of ovarian tissue grafted to CAM with avian erythrocytes detected in vessels from ovarian grafts on day 1 (**E**,**F**) and day 6 (**G**). Arrows point to ovarian grafts (**A-D**). Arrowheads indicate avian erythrocytes (**E-G**). Scale bar: 20 μm.

Hossay. Follicle outcomes in human ovarian tissue. Fertil Steril 2022.

50 μg/mL ascorbic acid [Sigma]), and placed in humidified air at 37°C with 5% CO_2 (20). On day 1, the culture medium was discarded and replaced with fresh medium supplemented with 10 ng/mL insulin (Sigma) and 1 ng/mL human follicle-stimulating hormone (FSH; Gonal F, Merck Serono, UK). Half of the fragments were cultured for an additional 5 days, with 50% of the medium replaced every 2 days, whereas the rest were harvested after 1 day of IVC.

CAM Model and Grafting Procedure

Fertilized day 0 eggs from Lohmann–selected-white Leghorn chickens were placed in an incubator (Polyhatch, Brinsea, Belgium) at 37°C in 40%–50% relative air humidity and rotated hourly. The eggs were incubated and processed as previously reported (33). On day 7 of egg incubation, 23 frozen-thawed cortical pieces ($4\times2\times1$ mm^3) were deposited onto traumatized CAM for 1 or 6 days (one piece per egg) (Fig. 1A). A small area of CAM was gently rubbed by touching it quickly with a 1-cm^2 strip of sterile ether-extracted lens paper, allowing the impenetrable upper peridermal part of its double epithelial layer to be removed (33). Three implants were excluded from further analysis because of embryo death ($n = 1$) or no tissue attachment to the CAM ($n = 2$), leading to tissue necrosis.

Histology

A total of 80 ovarian cortical pieces were fixed on day 0, 1, or 6 in 4% paraformaldehyde (2 fragments/patient/timepoint), embedded in paraffin and serially cut into 5-μm sections. Every eighth section was stained with hematoxylin and eosin (Merck, Germany), scanned by the Pannoramic P250 Flash III scanner (3DHISTECH, Hungary) at 20× magnification and analyzed with CaseViewer (v2.2).

Follicle outcomes. For follicle density and classification analyses, all follicles with a visible oocyte were counted in 12 sections per patient and per timepoint, and were at least 80 μm apart to avoid double counting and ensure an accurate representation of whole tissue blocks. Follicles were subsequently classified according to stage as primordial or growing (including primary, secondary, and antral follicles) (33). Total follicle density was then defined as the number of follicles per mm^3 (n/mm^3), calculating volume by multiplying digitized surfaces by fragment thickness. The percentage at each stage

was established for comparison between groups ($\frac{number\ of\ follicles\ per\ subgroup}{total\ number\ of\ follicles}$).

Graft revascularization. Reperfusion of implants grafted to CAM was assessed by identifying nucleated avian red blood cells in the lumen of blood vessels on hematoxylin and eosin-stained sections. The fact that these vessels were perfused demonstrates that they were mature and actively participating in tissue reoxygenation.

Immunohistochemistry

Slides were immunolabeled for Ki67 for proliferation assessment, cleaved caspase-3 for apoptosis, and microtubule-associated proteins 1A and 1B light chain 3B (LC3B) for autophagy, as well as markers of the PI3K pathway, including p-Akt, p-rpS6, and FOXO1. A detailed summary of the protocols can be found in Supplemental Table 1 (available online). Negative controls were obtained without incubating the primary antibody. One to 8 non-consecutive sections ($\geq$80 μm apart) were examined per patient and per timepoint, depending on the number of follicles present in the sections. Slides labeled with Ki67, caspase-3, or LC3B were analyzed with CaseViewer (v2.2). To assess PF proliferation rates, PFs were classified into 2 categories: resting, when all granulosa cells (GCs) were negative for Ki67 or proliferating, with at least 1 GC positive for Ki67 (34). For caspase-3 staining, follicles at all stages were evaluated and categorized as apoptotic when the oocyte and/or >50% of GCs were positive (35). For LC3B labeling, follicles were considered positive when the oocyte and/or GCs were stained with individual spots representing autophagosomes as a sign of prosurvival autophagy (36). However, strongly positive follicles characterized by multiple converging spots reflecting large numbers of autophagosomes leading to cell death were excluded from the analysis. Rates of follicle proliferation, apoptosis, and autophagy were assessed as a percentage of positive follicles out of total analyzed follicles. Sections labeled with p-Akt and p-rpS6 were investigated using QuPath software (v0.3.0) (37). After delineation and annotation of PFs, computer-assisted quantification of the stained area was achieved by applying the following formula: $x = \frac{positive\ area}{total\ area}$. Images of PFs stained with FOXO1 were analyzed using Fiji v1.52 (NIH, USA), as described elsewhere (38), with the red channel (WGA) serving to precisely delimit the cytoplasmic membrane of the oocyte and nuclear envelope. Results were expressed in a continuous dimension and calculated as: $x = \frac{mean\ intensity\ in\ nucleus}{mean\ intensity\ in\ nucleus\ and\ cytoplasm}$, with x >1 indicative of nuclear signaling (= follicle quiescence) and x <1 indicative of cytoplasmic signal localization (= follicle activation).

Droplet Digital PCR

Total ribonucleic acid (RNA) was extracted from formalin-fixed paraffin-embedded (FFPE) tissue sections. A detailed description of the extraction protocol can be found in Supplemental Material (available online). RNA purity and quantity were assured using the NanoDrop 2000c spectrophotometer (Thermo Scientific) and Qubit RNA BR assay (Thermo Fisher). All RNA samples were reverse transcribed at the same time using SuperScript IV VILO Master Mix (Invitrogen) and cDNA was stored at −80°C. FAM-labeled assays for PI3K pathway-related genes were *TSC1* (Hs01060648_m1) and *CDKN1B* (Hs00153277_m1), and for oocyte-related genes, *GDF9* (growth differentiation factor-9; Hs00193364_m1) and *LHX8* (LIM homoebox-8; Hs00418293_m1) (Applied Biosystems, Thermo Fisher Scientific, MA, USA) (39, 40). Each target gene assay was duplexed with and normalized to VIC-labeled assays for the Abelson 1 (ABL1) (Hs01104728_m1) (Applied Biosystems) reference gene using the QX200 Droplet Digital PCR (ddPCR) System (Bio-Rad Laboratories, Hercules, CA, USA). Preliminary compatibility tests were conducted to confirm duplexing suitability (data not shown). A detailed description of the ddPCR workflow is provided elsewhere (41). Negative (RNA extracted from FFPE ovarian tissue samples from a postmenopausal patient) and positive (RNA extracted from FFPE ovarian tissue samples from a premenopausal patient) control samples were inserted in each run, together with no template controls. Results were analyzed when the reference gene provided reliable amplification, gene expression levels were consistent between runs in control samples, and the number of tested droplets per well was $\geq$10,000.

Statistics

Statistical analyses for comparison of the different groups of patients (n = 5 per group) were conducted using GraphPad Prism software (v9.2 for Windows, USA). Timepoints within the same experimental group were first compared (= effect of time), before comparing groups with each other per timepoint (= effect of treatment). One-way ANOVA was used as a statistical test with Fisher's LSD post hoc in case of normal data distribution, including proportions after logit transformation. For data without normal distribution, the Kruskal-Wallis test was applied with the uncorrected Dunn's test post hoc. Results are expressed as mean ± SD. *P* values <.05 were considered statistically significant.

RESULTS

Chick Embryo Survival and Graft Vascularization Assessment

The overall survival rate of chick embryos was 95.6% (22 of 23 grafted eggs). After 1 day of grafting, all the fragments were already adherent to the CAM and showed a wheel-spoke pattern of blood vessels (10/10; Fig. 1B). By day 6, the implants were covered with a second layer of CAM, eventually becoming encapsulated, which led to even better vascularization of the grafts (Fig. 1C). Eighty percent of the transplants had also penetrated the egg (8/10; Fig. 1D), sometimes making it hard to retrieve them on day 6. Surprisingly, nucleated avian erythrocytes were observed in ovarian vessels of 30% of implants after only 1 day of transplantation (3/10) and in all implants by day 6, demonstrating a very rapid revascularization process (Fig. 1E–G).

Follicle Density and Classification

Total follicle density appeared to remain stable over time in all 3 groups, but tended to be higher in the FT-IVC group than the

FIGURE 2

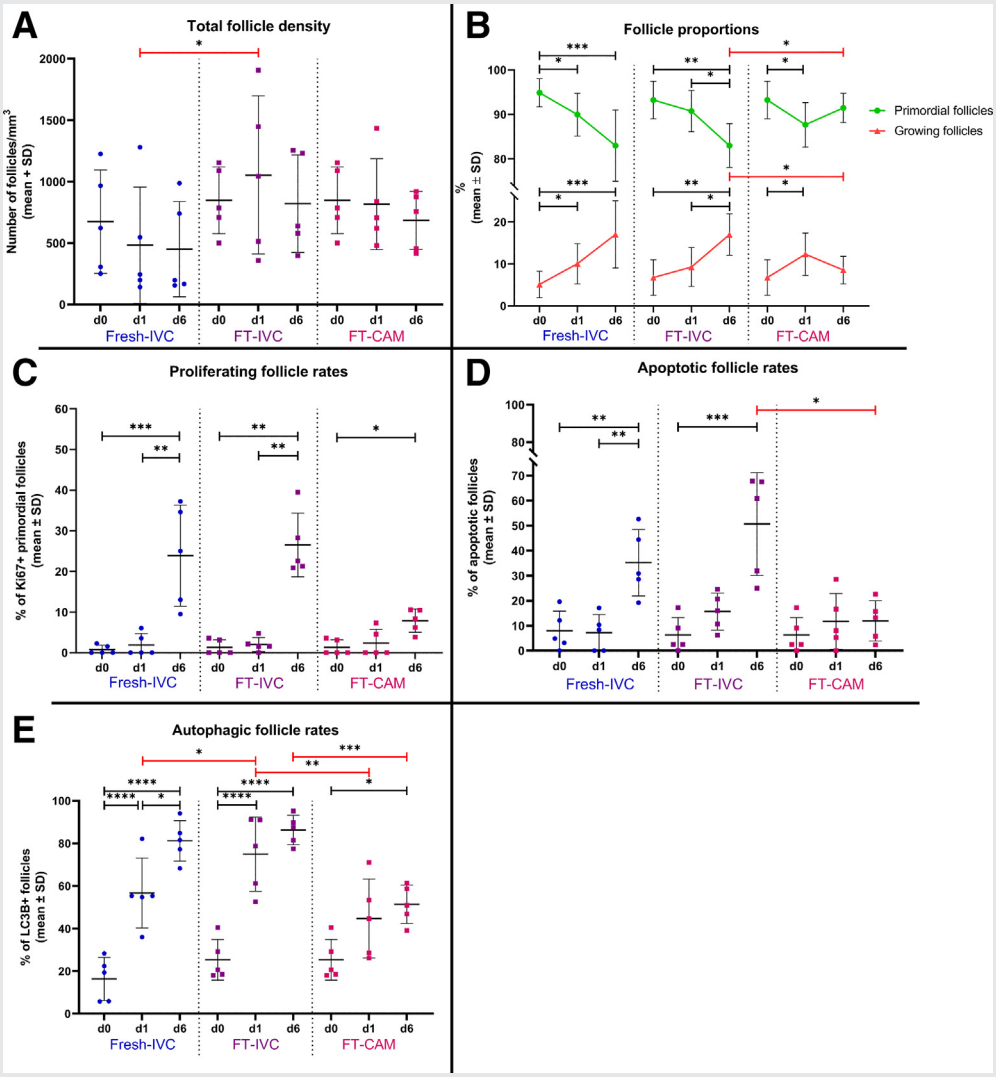

Follicle survival. (**A**) Total follicle density (number of follicles/mm^3 ± SD). (**B**) Proportion of primordial (*green dots*) and growing (*red triangles*) follicles out of total follicles ± SD. (**C**) Proliferating follicle rates (% of Ki67+ primordial follicles/total primordial follicles ± SD). (**D**) Apoptotic follicle rates (% of caspase-3+ follicles/total follicles ± SD). (**E**) Autophagic follicle rates (% of LC3B+ follicles/total follicles ± SD). Before undergoing any statistical analysis, results expressed as proportions (**B-E**) were logit-transformed. One-way ANOVA followed by *Fisher's LSD test* were applied for follicle density, proportions and autophagy (**A,B,E**). For follicle proliferation and apoptosis (**C,D**), the Kruskal-Wallis test followed by the uncorrected Dunn's test were used. *P* value reference: *P<.04, **P<.008, ***P<.001, ****P<.0001.

Hossay. Follicle outcomes in human ovarian tissue. Fertil Steril 2022.

fresh-IVC group, reaching significance on day 1 (1,054.50 ± 643.43 vs. 483.21 ± 472.70, P=.04) (Fig. 2A). Concerning the distribution of follicle stages, a considerable drop in PF rates was observed between days 0 and 6, in both the fresh-IVC (94.88 ± 3.17% vs. 82.98 ± 8%, P=.0003) and FT-IVC (93.23 ± 4.21% vs. 82.99 ± 4.93%, P=.002) groups, correlating with a significant increase in growing follicle rates in the fresh-IVC (5.12 ± 3.17% vs. 17.02 ± 8%, P=.0003) and FT-IVC (6.77 ± 4.21% vs. 17.01 ± 4.93%, P=.002) groups (Fig. 2B). In the FT-CAM group, a temporary decline was detected in PF rates between days 0 and 1 (93.23 ± 4.21% vs. 87.67 ± 5.02%, P=.04), which was associated with a short-lived upturn in growing follicle rates (6.77 ± 4.21% vs. 12.3 ± 5.02%, P=.04). Primordial and growing follicle rates then returned to initial levels on day 6 (vs. d0, P>.05), with the proportion of PFs remaining notably higher than in the FT-IVC group (91.46 ± 3.29% vs. 82.99 ± 8%, P=.03). No difference was identified between the fresh-IVC and FT-IVC groups.

Follicle Survival

In both the fresh-IVC and FT-IVC groups, proportions of Ki67-positive PFs were significantly greater on day 6 (23.88

FIGURE 3

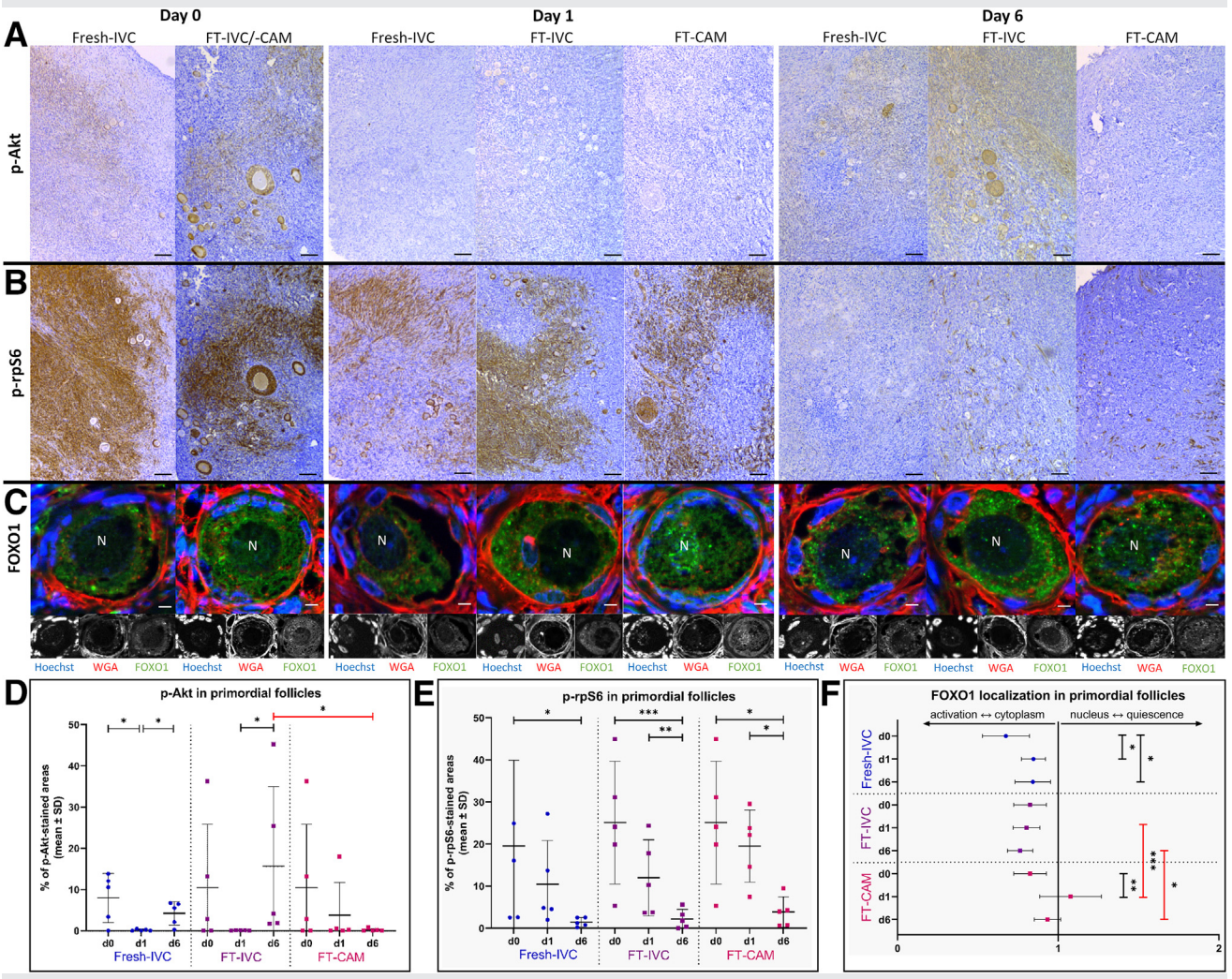

PI3K pathway-related follicle activation. (**A**) p-Akt immunostaining. (**B**) p-rpS6 immunolabeling. (**C**) FOXO1 immunofluorescent staining in primordial follicles (*green color*). (**D**) Proportion of p-Akt-stained surface area in primordial follicles evaluated by the Kruskal-Wallis test and the uncorrected Dunn's post hoc test after logit transformation. (**E**) Proportion of p-rpS6-positive surface area in primordial follicles assessed by one-way ANOVA and Fisher's LSD post hoc test after logit transformation. (**F**) FOXO1 localization analysis (nuclear mean intensity staining/total mean intensity staining ± SD) in primordial follicles evaluated by one-way ANOVA followed by Fisher's LSD post hoc test. N: oocyte nucleus. WGA: wheat germ agglutinin. Scale bars: 100 μm (**A–B**), 5 μm (**C**). *P* value reference: **P*<.05, ***P*<.004, ****P*<.0007.

Hossay. Follicle outcomes in human ovarian tissue. Fertil Steril 2022.

± 12.43% and 26.50 ± 7.83%) compared with day 0 controls (0.77 ± 1.08%, *P*=.001, and 1.34 ± 1.84%, *P*=.001) and day 1 (1.93 ± 2.78%, *P*=.003, and 2 ± 1.73%, *P*=.005) respectively (Fig. 2C). No significant difference was encountered between the fresh-IVC and FT-IVC groups. In the FT-CAM group, proliferating follicle rates were slightly higher on day 6 (7.89 ± 2.87%) compared with day 0 controls (1.34 ± 1.84%, *P*=.04), but were still 3 times lower than in the FT-IVC group (26.50 ± 7.83%, *P*>.05).

With regard to apoptotic follicle rates, a considerable increase was seen in the proportion of caspase-3-positive follicles in the fresh-IVC and FT-IVC groups on day 6 (35.16 ± 13.29% and 50.66 ± 20.57%) compared with day 0 (7.95 ± 7.89%, *P*=.008, and 6.27 ± 7%, *P*=.0008) and day 1 (7.16 ± 7.31%, *P*=.005, and 15.64 ± 7.38%, *P*=.05), respectively (Fig. 2D). However, in the FT-CAM group no significant increase was observed (d0: 6.27 ± 7% vs. d6: 11.92 ± 8.05%, *P*>.05), with apoptotic follicle rates remaining substantially lower than in the FT-IVC group on day 6 (50.66 ± 20.57%, *P*=.01). No significant difference was observed between the fresh-IVC and FT-IVC groups.

In terms of autophagic follicle rates, a significant increase was noted in proportions of LC3B-positive follicles in the fresh-IVC and FT-IVC groups on days 1 (56.71 ± 16.46%, *P*<.0001, and 74.95 ± 17.48%, *P*<.0001) and 6 (81.22 ± 9.52%, *P*<.0001, and 86.29 ± 6.96%, *P*<.0001) compared with day 0 controls (16.34 ± 10.13% and 25.35 ± 9.55%), respectively (Fig. 2E). Moreover, levels were slightly higher

TABLE 1

Gene expression levels in ovarian tissue sections

Genes		Condition			
		Day 0	Day 1	Day 6	*P* value reference
GDF9	Fresh-IVC	0.03 ± 0.02	0.02 ± 0.02[c]	0.04 ± 0.03[d]	[c]*P*=.03; [d]*P*=.04
	FT-IVC	0.07 ± 0.03	0.06 ± 0.06[c]	0.11 ± 0.07[d]	
	FT-CAM	0.07 ± 0.03	0.04 ± 0.02	0.04 ± 0.03	
LHX8	Fresh-IVC	0.13 ± 0.073	0.06 ± 0.07[c]	0.06 ± 0.05[d]	[c]*P*=.03; [d]*P*=.02
	FT-IVC	0.31 ± 0.13	0.22 ± 0.19[c]	0.17 ± 0.08[d]	
	FT-CAM	0.31 ± 0.13[a,b]	0.11 ± 0.06[a]	0.11 ± 0.08[b]	[a]*P*<.05; [b]*P*=.03
TSC1	Fresh-IVC	0.70 ± 0.04[a,b]	0.18 ± 0.04[a]	0.31 ± 0.08[b]	[a]*P*=.0001; [b]*P*=.02
	FT-IVC	0.81 ± 0.05[a,b]	0.23 ± 0.03[a]	0.39 ± 0.09[b]	[a]*P*=.0002; [b]*P*<.05
	FT-CAM	0.81 ± 0.05[a]	0.27 ± 0.07[a]	0.42 ± 0.05	[a]*P*=.001
CDKN1B	Fresh-IVC	2.01 ± 0.19[a,b]	0.57 ± 0.10[a]	0.65 ± 0.14[b]	[a]*P*=.0003; [b]*P*=.002
	FT-IVC	1.60 ± 0.21[a]	0.56 ± 0.06[a]	0.80 ± 0.15	[a]*P*=.0009
	FT-CAM	1.60 ± 0.21[a]	0.63 ± 0.18[a]	0.85 ± 0.17	[a]*P*=.006

Note: Statistical analysis was performed using the Kruskal-Wallis test followed by the uncorrected Dunn's test. The same superscript letters ([a,b]) indicate statistically significant differences over time in a specific group, and the same superscript letters ([c,d]) represent statistically significant differences between groups. GDF9 = growth differentiation factor-9; LHX8 = LIM homoebox-8; TSC1 = tuberous sclerosis complex 1; CDKN1B = cyclin-dependent kinase inhibitor 1B; IVC = in vitro culture; CAM = chorioallantoic membrane; FT = frozen-thawed.

Hossay. Follicle outcomes in human ovarian tissue. Fertil Steril 2022.

in the FT-IVC group than the fresh-IVC on day 1 (P=.04). In the FT-CAM group, autophagic follicle rates were higher on day 6 (51.38 ± 9.02%) than on day 0 (25.35 ± 9.55%, P=.02), but remained significantly lower than in the FT-IVC group on days 1 (44.75 ± 18.54% vs. 74.95 ± 17.48%, P=.003) and 6 (51.38 ± 9.02% vs. 86.29 ± 6.96%, P=.0003), respectively.

PI3K Pathway-Related Follicle Activation

p-Akt. A total of 345 PFs were investigated for the p-Akt marker in the fresh-IVC group, 352 in the FT-IVC group, and 348 in the FT-CAM group (Fig. 3A and D). Percentages of p-Akt-stained areas decreased in all groups on day 1, reaching statistical significance in the fresh-IVC group (d0: 7.97 ± 5.97% vs. d1: 0.16 ± 0.22%, P<.05). This decline in the proportion of stained areas on day 1 was followed by a significant increase on day 6 in the fresh-IVC (d1: 0.16 ± 0.22% vs. d6: 4.24 ± 2.88%, P<.05) and FT-IVC (d1: 0.08 ± 0.07% vs. d6: 15.68 ± 19.29%, P=.01) groups. Conversely, in the FT-CAM group, the falling trend in the proportion of p-Akt-stained areas on day 1 (3.78 ± 7.96%) continued its decline to day 6 (0.22 ± 0.34%), and was significantly lower than in the FT-IVC group (d6: 15.68 ± 19.29%, P=.02). Freezing did not affect p-Akt modulation in PFs, as no significant differences were seen between the fresh-IVC and FT-IVC groups.

p-rpS6. A total of 408 PFs were investigated for the p-rpS6 marker in the fresh-IVC group, 477 in the FT-IVC group, and 392 in the FT-CAM group (Fig. 3B and E). Percentages of p-rpS6-stained areas fell by around 20% in all groups by day 6 compared with day 0 controls, reaching statistical significance in all 3 (fresh-IVC d0: 7.97 ± 5.97% vs. d6: 0.16 ± 0.22%, P=.02; FT-IVC d0: 25.11 ± 14.59% vs. d6: 2.19 ± 2.3%, P=.03; and FT-CAM d0: 25.11 ± 14.59% vs. d6: 3.84 ± 3.6%, P=.04). No difference was observed between any of the groups.

FOXO1. A total of 276 PFs were investigated for the FOXO1 marker in the fresh-IVC group, 352 in the FT-IVC group, and 264 in the FT-CAM group (Fig. 3C and F). FOXO1 was mainly found in the cytoplasm of oocytes on day 0 in all groups, maintaining its cytoplasmic location in the fresh-IVC and FT-IVC groups over time. Although FOXO1 remained cytoplasmic through days 1 (0.85 ± 0.07) to 6 (0.84 ± 0.11) in the fresh-IVC group, its cytoplasmic presence was most pronounced on day 0 (0.67 ± 0.15; vs. d1 P=.03; vs. d6 P=.03). A significant cytoplasm-to-nucleus shift was detected in the FT-CAM group on day 1 (1.08 ± 0.19) compared with day 0 controls (0.82 ± 0.1, P=.002). Moreover, FOXO1 was also significantly more nuclear in the FT-CAM group than in the FT-IVC group on days 1 (1.08 ± 0.19 vs. 0.8 ± 0.08, P=.0007) and 6 (0.93 ± 0.08 vs. 0.76 ± 0.08, P=.03) respectively. Once again, the PI3K pathway in PFs was not impacted by freezing.

Gene Expression in Ovarian Tissue

Oocyte-related genes. The expression levels of gene *GDF9* suggested triggering of oocyte growth in fresh-IVC and FT-IVC tissues, trending towards higher values by day 6 compared with day 1 (Table 1). On the other hand, a non-significant decrease was observed in the FT-CAM group on days 1 and 6 compared with day 0, suggesting that oocyte growth was not induced in this group.

On the other hand, *LHX8* is a known transcription factor specifically expressed by oocytes, presumably playing a role in early follicle stages by inhibiting follicle autophagy (42–44). The expression levels of *LHX8* dropped in all groups, but only reached statistical significance in the FT-CAM group (d0 vs. d1, P<.05; d0 vs. d6, P=.03).

Interestingly, *GDF9* and *LHX8* expression levels seemed higher in the FT-IVC group than in the fresh-IVC group and were statistically significant on days 1 and 6 (P<.04). This may be explained by higher follicle numbers in the FT-IVC group.

PI3K pathway-related genes. Expression levels of *TSC1* and *CDKN1B* in ovarian tissues followed the same pattern in all

groups, with a significant decrease on day 1 compared with day 0 controls ($P < .006$) (Table 1). On day 6, they remained as low as on day 1, with no differences detected between any of the groups.

DISCUSSION

The aim of the present study was to investigate the potential causes of PF pool depletion in cryopreserved human ovarian tissue. We looked into the impact of freezing, IVC, and grafting to CAM on follicle dynamics by assessing various molecular pathways involved in activation, apoptosis, and autophagy.

Follicle Development

Higher rates of follicle proliferation and apoptosis were demonstrated in both fresh-IVC and FT-IVC tissues, confirming that follicle depletion occurs through initiation of follicle activation and death (9, 10), with no impact of slow-freezing (8, 21–23). Our findings appear to indicate that IVC itself is enough to cause significant follicle activation and apoptosis (20, 24, 45–47). On the contrary, when grafted to CAM, human frozen-thawed ovarian tissue did not exhibit any follicle activation, as reflected by comparable PF proportions on days 0 and 6, and decreasing *GDF9* gene expression levels over time. Furthermore, no increase in apoptotic follicle rates was seen in this group. All in all, these results point to a protective effect of CAM on the human ovarian reserve, which is in line with previous studies using ovarian tissue from different animal models (28–31).

PI3K Pathway-Related Follicle Activation

Our results show that the onset of follicle activation during IVC is driven by upregulation of the PI3K/Akt/FOXO pathway, as previously demonstrated in xenografting experiments (10, 38, 48). We established that the absence of follicle activation in the FT-CAM group was related to significant downregulation of the *PI3K/Akt/FOXO* pathway, with significantly lower p-Akt levels and also significant cytoplasm-to-nucleus shifts in FOXO1 in PFs compared with the FT-IVC group. These findings further highlight the central involvement of FOXO1 in regulating oocyte-mediated activation in PFs (49, 50).

Upon greater scrutiny of the phosphorylation patterns of Akt, the PF pool appeared to have undergone multi-wave PI3K pathway upregulation. We hypothesize that a first wave of activation may be triggered by removal of ovarian tissue from its physiological environment and processing of the biopsy, as already suggested by studies investigating the role of PI3K and Hippo pathways in ovarian tissue (15, 47). Indeed, we noted that when the tissue was fixed immediately upon surgical removal, Akt remained unphosphorylated in PFs (data not shown). However, when we took the time required for biopsy preparation for IVC or grafting, Akt phosphorylation levels clearly spiked (= d0), presumably leading to the first activation wave. It is worth pointing out that our experiment proved that cryopreservation by slow-freezing has no additional impact on this first event. A delayed second wave then results from IVC itself (20, 24, 45–47). Efforts should therefore focus on how to exploit the PI3K/Akt/FOXO pathway, taking into account its diverse modulation during ovarian cortical strip preparation and IVC. The PI3K pathway also appeared to be differently regulated in whole tissue than in follicles, making it challenging to obtain conclusive results when investigating ubiquitous signaling in tissue as heterogeneous as the ovary.

Follicle Autophagy

To further assess the pro-survival follicle response to stressful events, we evaluated autophagy in follicles (18, 36), which was found to increase in all groups. Nonetheless, levels remained much lower in the FT-CAM group, reflecting the less stress-inducing nature of the procedure. Autophagy has also been shown to be suppressed by mTOR (18). Downregulation of mTOR activity was observed over time in our data through a decline in p-rpS6 levels in PFs in all groups, suggesting inhibition of mTOR activity potentially resulting in enhanced follicle autophagy, as encountered in the present study. The balance in favor of the latter promotes follicle survival through a number of different functions, including metabolism, energy production, and cell death regulation (18, 36). Further proof of the involvement of autophagy in ovarian tissue survival was provided by *LHX8* gene expression levels. Our findings appear to confirm the role of *LHX8* in the regulation of oocyte autophagy in humans, having found it to be increasingly downregulated in all groups over time.

Protective Role of CAM

The protective role of CAM in preservation of the PF pool may be explained by 2 distinct mechanisms with potentially synergistic effects. The first is the swift revascularization of ovarian grafts, as evidenced by the presence of avian red blood cells from the first day of grafting. Revascularization is much slower when grafting ovarian tissue onto the peritoneum of immunodeficient mice, occurring only from day 5 onwards (51). This delay is known to be one of the major causes of follicle loss, whereas promoting rapid revascularization after transplantation results in better PF pool survival (52–56).

The second mechanism that may be involved is antimüllerian hormone (AMH), which plays a known role in regulation of follicle growth and maintenance of homeostasis of the preantral follicle reserve. The gonads of chick embryos of both sexes produce this hormone. It was suggested that circulating embryonic AMH participates in downregulating follicle activation in CAM-grafted bovine ovarian grafts, where follicle activation was re-established when chick embryos were gonadectomized (30). Administration of AMH was also recently found to curb PF activation and loss induced by chemotherapy regimens (57–59). Nevertheless, the impact of AMH on follicle activation remains contentious in primates, suggesting overall that AMH may act as an inhibitor or stimulator of follicle growth in a species-specific, age-specific (fetal/newborn vs. adult) and dose-dependent manner (33, 60–63).

CONCLUSION

Based on our findings and data from the literature, we can confirm that slow-freezing is a satisfactory means of ovarian tissue cryopreservation, with no impact on early follicle dynamics in terms of growth, survival, or stress-related response by activation of autophagy. However, PF pool depletion did occur during IVC through both PF activation due to upregulation of the PI3K/Akt/FOXO pathway and increased follicle apoptosis. Grafting to CAM was able to counteract these events by inhibiting PF activation and reducing apoptotic follicle rates, presumably thanks to rapid graft revascularization and/or a probable role of circulating embryonic AMH, as suggested in the literature. These findings should actively encourage further research efforts to enhance neoangiogenesis in ovarian grafts and investigate the potential benefits of administering AMH to avoid PF burnout, possibly as a combined strategy.

Acknowledgments: The authors thank Mira Hryniuk, B.A., for reviewing the English language of the article and Dolores Gonzalez, Olivier Van Kerk, and Sarah Storder for their technical assistance. The authors also warmly thank Prof. Pascale Saussoy and Joachim Ravau for sharing their knowledge on ddPCR.

REFERENCES

1. Donnez J, Dolmans MM. Fertility preservation in women. N Engl J Med 2017;377:1657–65.
2. Shapira M, Dolmans MM, Silber S, Meirow D. Evaluation of ovarian tissue transplantation: results from three clinical centers. Fertil Steril 2020;114:388–97.
3. Dolmans MM, Hossay C, Nguyen TYT, Poirot C. Fertility preservation: How to preserve ovarian function in children, adolescents and adults. J Clin Med 2021;10:5247.
4. Dolmans MM, Donnez J, Cacciottola L. Fertility preservation: the challenge of freezing and transplanting ovarian tissue. Trends Mol Med 2021;27:777–91.
5. Gosden RG, Baird DT, Wade JC, Webb R. Restoration of fertility to oophorectomized sheep by ovarian autografts stored at-196°C. Hum Reprod 1994;9:597–603.
6. Baird DT, Webb R, Campbell BK, Harkness LM, Gosden RG. Long-term ovarian function in sheep after ovariectomy and transplantation of autografts stored at −196 C. Endocrinology 1999;140:462–71.
7. Aubard Y, Piver P, Cogni Y, Fermeaux V, Poulin N, Driancourt MA. Orthotopic and heterotopic autografts of frozen–thawed ovarian cortex in sheep. Hum Reprod 1999;14:2149–54.
8. Nisolle M, Casanas-Roux F, Qu J, Motta P, Donnez J. Histologic and ultrastructural evaluation of fresh and frozen-thawed human ovarian xenografts in nude mice. Fertil Steril 2000;74:122–9.
9. Gavish Z, Spector I, Peer G, Schlatt S, Wistuba J, Roness H, et al. Follicle activation is a significant and immediate cause of follicle loss after ovarian tissue transplantation. J Assist Reprod Genet 2018;35:61–9.
10. Masciangelo R, Hossay C, Donnez J, Dolmans MM. Does the Akt pathway play a role in follicle activation after grafting of human ovarian tissue? Reprod Biomed Online 2019;39:196–8.
11. Gougeon A, Chainy GBN. Morphometric studies of small follicles in ovaries of women at different ages. J Reprod Fertil 1987;81:433–42.
12. Picton HM, Harris SE, Muruvi W, Chambers EL. The in vitro growth and maturation of follicles. Reproduction 2008;136:703–15.
13. Wallace WHB, Kelsey TW. Human ovarian reserve from conception to the menopause. PLoS One 2010;5:e8772.
14. Roness H, Meirow D. FERTILITY PRESERVATION: Follicle reserve loss in ovarian tissue transplantation. Reproduction 2019;158:F35–44.
15. Kawamura K, Cheng Y, Suzuki N, Deguchi M, Sato Y, Takae S, et al. Hippo signaling disruption and Akt stimulation of ovarian follicles for infertility treatment. Proc Natl Acad Sci U S A 2013;110:17474–9.
16. Hsueh AJW, Kawamura K, Cheng Y, Fauser BCJM. Intraovarian control of early folliculogenesis. Endocr Rev 2015;36:1–24.
17. Zhang H, Liu K. Cellular and molecular regulation of the activation of mammalian primordial follicles: somatic cells initiate follicle activation in adulthood. Hum Reprod Update 2015;21:779–86.
18. Zhou J, Peng X, Mei S. Autophagy in ovarian follicular development and atresia. Int J Biol Sci 2019;15:726–37.
19. Song ZH, Yu HY, Wang P, Mao GK, Liu WX, Li MN, et al. Germ cell-specific Atg7 knockout results in primary ovarian insufficiency in female mice. Cell Death Dis 2015;6:e1589–e1589.
20. Grosbois J, Demeestere I. Dynamics of PI3K and Hippo signaling pathways during in vitro human follicle activation. Hum Reprod 2018;33:1705–14.
21. Schubert B, Canis M, Darcha C, Artonne C, Smitz J, Grizard G. Follicular growth and estradiol follow-up after subcutaneous xenografting of fresh and cryopreserved human ovarian tissue. Fertil Steril 2008;89:1787–94.
22. Amorim CA, David A, Dolmans MM, Camboni A, Donnez J, Van Langendonckt A. Impact of freezing and thawing of human ovarian tissue on follicular growth after long-term xenotransplantation. J Assist Reprod Genet 2011;28:1157–65.
23. David A, Dolmans MM, Van Langendonckt A, Donnez J, Amorim CA. Immunohistochemical localization of growth factors after cryopreservation and 3 weeks' xenotransplantation of human ovarian tissue. Fertil Steril 2011;95:1241–6.
24. Terren C, Nisolle M, Munaut C. Pharmacological inhibition of the PI3K/PTEN/Akt and mTOR signalling pathways limits follicle activation induced by ovarian cryopreservation and in vitro culture. J Ovarian Res 2021;14:95.
25. Giannopoulou E, Katsoris P, Hatziapostolou M, Kardamakis D, Kotsaki E, Polytarchou C, et al. X-rays modulate extracellular matrixin vivo. Int J Cancer 2001;94:690–8.
26. Witz CA, Montoya-Rodriguez IA, Cho S, Centonze VE, Bonewald LF, Schenken RS. Composition of the extracellular matrix of the peritoneum. J Soc Gynecol Investig 2001;8:299–304.
27. Dolmans MM, von Wolff M, Poirot C, Diaz-Garcia C, Cacciottola L, Boissel N, et al. Transplantation of cryopreserved ovarian tissue in a series of 285 women: a review of five leading European centers. Fertil Steril 2021;115:1102–15.
28. Fortune JE, Cushman RA, Wahl CM, Kito S. The primordial to primary follicle transition. Mol Cell Endocrinol 2000;163:53–60.
29. Cushman RA, Wahl CM, Fortune JE. Bovine ovarian cortical pieces grafted to chick embryonic membranes: a model for studies on the activation of primordial follicles. Hum Reprod 2002;17:48–54.
30. Gigli I, Cushman RA, Wahl CM, Fortune JE. Evidence for a role for antimüllerian hormone in the suppression of follicle activation in mouse ovaries and bovine ovarian cortex grafted beneath the chick chorioallantoic membrane: FOLLICLE ACTIVATION AND AMH. Mol Reprod Dev 2005;71:480–8.
31. Qureshi AI, Nussey SS, Bano G, Musonda P, Whitehead SA, Mason HD. Testosterone selectively increases primary follicles in ovarian cortex grafted onto embryonic chick membranes: relevance to polycystic ovaries. Reproduction 2008;136:187–94.
32. Dolmans MM, Jadoul P, Gilliaux S, Amorim CA, Luyckx V, Squifflet J, et al. A review of 15 years of ovarian tissue bank activities. J Assist Reprod Genet 2013;30:305–14.
33. Martinez-Madrid B, Donnez J, Van Eyck AS, Veiga-Lopez A, Dolmans MM, Van Langendonckt A. Chick embryo chorioallantoic membrane (CAM) model: a useful tool to study short-term transplantation of cryopreserved human ovarian tissue. Fertil Steril 2009;91:285–92.
34. Luyckx V, Scalercio S, Jadoul P, Amorim CA, Soares M, Donnez J, et al. Evaluation of cryopreserved ovarian tissue from prepubertal patients after long-term xenografting and exogenous stimulation. Fertil Steril 2013;100:1350–7.
35. Amorim CA, Donnez J, Dehoux JP, Scalercio SR, Squifflet J, Dolmans MM. Long-term follow-up of vitrified and autografted baboon (*Papio anubis*) ovarian tissue. Hum Reprod 2019;34:323–34.

36. Peters AE, Caban SJ, McLaughlin EA, Roman SD, Bromfield EG, Nixon B, et al. The Impact of aging on macroautophagy in the pre-ovulatory mouse oocyte. Front Cell Dev Biol 2021;9:691826.
37. Bankhead P, Loughrey MB, Fernández JA, Dombrowski Y, McArt DG, Dunne PD, et al. QuPath: open source software for digital pathology image analysis. Sci Rep 2017;7:16878.
38. Cacciottola L, Courtoy GE, Nguyen TYT, Hossay C, Donnez J, Dolmans MM. Adipose tissue-derived stem cells protect the primordial follicle pool from both direct follicle death and abnormal activation after ovarian tissue transplantation. J Assist Reprod Genet 2021;38:151–61.
39. Aaltonen J, Laitinen MP, Vuojolainen K, Jaatinen R, Horelli-Kuitunen N, Seppä L, et al. Human growth differentiation factor 9 (GDF-9) and its novel homolog GDF-9B are expressed in oocytes during early folliculogenesis. J Clin Endocrinol Metab 1999;84:2744–50.
40. White YAR, Woods DC, Takai Y, Ishihara O, Seki H, Tilly JL. Oocyte formation by mitotically active germ cells purified from ovaries of reproductive-age women. Nat Med 2012;18:413–21.
41. Nguyen TYT, Cacciottola L, Camboni A, Ravau J, De Vos M, Demeestere I, et al. Ovarian tissue cryopreservation and transplantation in patients with central nervous system tumours. Hum Reprod 2021;36:1296–309.
42. Ren Y, Suzuki H, Jagarlamudi K, Golnoski K, McGuire M, Lopes R, et al. Lhx8 regulates primordial follicle activation and postnatal folliculogenesis. BMC Biol 2015;13:39.
43. Kristensen SG, Ebbesen P, Andersen CY. Transcriptional profiling of five isolated size-matched stages of human preantral follicles. Mol Cell Endocrinol 2015;401:189–201.
44. D'Ignazio L, Michel M, Beyer M, Thompson K, Forabosco A, Schlessinger D, et al. Lhx8 ablation leads to massive autophagy of mouse oocytes associated with DNA damage. Biol Reprod 2018;98:532–42.
45. Telfer EE, McLaughlin M, Ding C, Thong KJ. A two-step serum-free culture system supports development of human oocytes from primordial follicles in the presence of activin. Hum Reprod 2008;23:1151–8.
46. McLaughlin M, Kinnell HL, Anderson RA, Telfer EE. Inhibition of phosphatase and tensin homologue (PTEN) in human ovary in vitro results in increased activation of primordial follicles but compromises development of growing follicles. Mol Hum Reprod 2014;20:736–44.
47. Devos M, Grosbois J, Demeestere I. Interaction between PI3K/AKT and Hippo pathways during in vitro follicular activation and response to fragmentation and chemotherapy exposure using a mouse immature ovary model. Biol Reprod 2020;102:717–29.
48. Masciangelo R, Hossay C, Chiti MC, Manavella DD, Amorim CA, Donnez J, et al. Role of the PI3K and Hippo pathways in follicle activation after grafting of human ovarian tissue. J Assist Reprod Genet 2020;37:101–8.
49. Castrillon DH, Miao L, Kollipara R, Horner JW, DePinho RA. Suppression of ovarian follicle activation in mice by the transcription factor Foxo3a. Science 2003;301:215–8.
50. Liu L, Rajareddy S, Reddy P, Du C, Jagarlamudi K, Shen Y, et al. Infertility caused by retardation of follicular development in mice with oocyte-specific expression of Foxo3a. Development 2007;134:199–209.
51. Van Eyck A-S, Bouzin C, Feron O, Romeu L, Van Langendonckt A, Donnez J, et al. Both host and graft vessels contribute to revascularization of xenografted human ovarian tissue in a murine model. Fertil Steril 2010;93:1676–85.
52. Cacciottola L, Donnez J, Dolmans MM. Ovarian tissue damage after grafting: systematic review of strategies to improve follicle outcomes. Reprod Biomed Online 2021;43:351–69.
53. Israely T, Nevo N, Harmelin A, Neeman M, Tsafriri A. Reducing ischaemic damage in rodent ovarian xenografts transplanted into granulation tissue. Hum Reprod 2006;21:1368–79.
54. Shikanov A, Zhang Z, Xu M, Smith RM, Rajan A, Woodruff TK, et al. Fibrin encapsulation and vascular endothelial growth factor delivery promotes ovarian graft survival in mice. Tissue Eng Part A 2011;17:3095–104.
55. Soleimani R, Heytens E, Oktay K. Enhancement of neoangiogenesis and follicle survival by sphingosine-1-phosphate in human ovarian tissue xenotransplants. PLoS One 2011;6:e19475.
56. Tanaka A, Nakamura H, Tabata Y, Fujimori Y, Kumasawa K, Kimura T. Effect of sustained release of basic fibroblast growth factor using biodegradable gelatin hydrogels on frozen-thawed human ovarian tissue in a xenograft model. J Obstet Gynaecol Res 2018;44:1947–55.
57. Kano M, Sosulski AE, Zhang L, Saatcioglu HD, Wang D, Nagykery N, et al. AMH/MIS as a contraceptive that protects the ovarian reserve during chemotherapy. Proc Natl Acad Sci U S A 2017;114:E1688–97.
58. Roness H, Spector I, Leichtmann-Bardoogo Y, Savino AM, Dereh-Haim S, Meirow D. Pharmacological administration of recombinant human AMH rescues ovarian reserve and preserves fertility in a mouse model of chemotherapy, without interfering with anti-tumoural effects. J Assist Reprod Genet 2019;36:1793–803.
59. Sonigo C, Beau I, Grynberg M, Binart N. AMH prevents primordial ovarian follicle loss and fertility alteration in cyclophosphamide-treated mice. FASEB J 2019;33:1278–87.
60. Carlsson IB, Scott JE, Visser JA, Ritvos O, Themmen AP, Hovatta O. Antimullerian hormone inhibits initiation of growth of human primordial ovarian follicles in vitro. Hum Reprod 2006;21:2223–7.
61. Man L, Park L, Bodine R, Ginsberg M, Zaninovic N, Man OA, et al. Engineered endothelium provides angiogenic and paracrine stimulus to grafted human ovarian tissue. Sci Rep 2017;7:8203.
62. Detti L, Fletcher NM, Saed GM, Sweatman TW, Uhlmann RA, Pappo A, et al. Xenotransplantation of pre-pubertal ovarian cortex and prevention of follicle depletion with antimullerian hormone (AMH). J Assist Reprod Genet 2018;35:1831–41.
63. Schmidt KLT, Kryger-Baggesen N, Byskov AG, Andersen CY. Antimullerian hormone initiates growth of human primordial follicles in vitro. Mol Cell Endocrinol 2005;234:87–93.

Resultados de folículos en tejido ovárico humano: efecto del congelamiento, cultivo y trasplante.

Objetivo: Estudiar el efecto del congelamiento, cultivo in vitro (IVC) y trasplante en la membrana corioalantoidea (CAM) sobre los resultados de folículos en tejido ovárico humano.

Diseño: Estudio experimental.

Escenario: Laboratorio Universitario de investigación básica.

Pacientes: El tejido ovárico fresco y criopreservado de 10 pacientes fueron donados para investigación con su consentimiento y aprobación por el comité de revisión institucional.

Intervención: Se compararon piezas de corteza ovárica cultivadas in vitro en fresco (Fresco-IVC) y cultivadas in vitro luego de congelamiento-descongelamiento (FT-IVC).
Los fragmentos FT-IVC fueron luego evaluados contra fragmentos trasplantados en CAM (FT-CAM). Los trasplantes de piezas corticales de ovario (421 mm) de IVC y CAM fueron analizados en los días 0, 1 y 6.

Medición de resultado principal: El análisis folicular incluyó la histología (conteo y clasificación) e inmunohistoquímica (Ki67 [proliferación], caspasa 3 [apoptosis], cadena ligera 3B de proteínas 1A y 1B [autofagia], p-Akt, FOXO1 y p-rpS6 [activación PI3K]). Posteriormente se usó PCR digital para la explorar de la expresión de la vía PI3K- y genes relacionados a ovocitos de las secciones ováricas.

Resultados: No se encontraron mayores diferencias entre tejidos fresco-IVC y FT-IVC en ninguno de los análisis realizados. Aunque se observó una disminución significativa de la proporción de folículos primordiales (PF) en los grupos fresco-IVC y FT-IVC (d0 vs. D6, $P<.002$), estos se mantuvieron estables en el grupo FT-CAM (d0 vs. D6, ns). Las tasas de PF fueron significativamente mayores en el grupo FT-CAM en comparación al grupo FT-IVC en d6 (P1/4.02).
De forma importante, eritrocitos aviares se encontraban presentes en un 30% de los trasplantes desde d1. Las tasas de apoptosis y autofagia incrementaron durante IVC ($P<.008$), pero se mantuvieron significativamente bajas en el grupo FT-CAM ($P<.01$), confirmando una mejor preservación en los trasplantes de tejidos CAM. Se estableció una regulación río arriba de la vía PI3K/FOXO en los grupos IVC, demostrando una activación PF, mientras que se detectó una regulación río abajo en el grupo FT-CAM ($P<.03$). La prueba de PCR confirmó el crecimiento ovocitario durante la IVC y la autofagia folicular en todos los grupos, sin embargo, la vía PI3K parecía estar modulada diferencialmente en tejidos y folículos.

Conclusión: El cultivo in vitro induce a la depleción de PF sin un impacto adicional del congelamiento. Injertar en CAM mantiene el conjunto de PF frenando la activación folicular, apoptosis, y autofagia, probablemente gracias a la rápida re-vascularización y/o a la hormona anti-mulleriana embrionaria circulante.
Estos hallazgos resaltan la importancia de mejorar la neo-angiogénesis en los trasplantes de ovario e investigar los potenciales beneficios de administrar la hormona anti-mulleriana para prevenir el agotamiento de PF.